8

Modeling and Simulation of Chemical System Vaporization at High Temperature: Application to the Vitrification of Fly Ashes and Radioactive Wastes by Thermal Plasma

Imed Ghiloufi
College of Sciences, Department of Physics,
Al-Imam Muhammad Ibn Saud University, Riyadh,
Kingdom of Saudi Arabia

1. Introduction

The treatment, at high temperatures, of such chemical systems as the fly ashes and radioactive wastes requires the control of its element volatility. Precisely, it requires following the evolution of the system during treatment and determining the composition of the system in all phases.

For a closed chemical system, the calculation of its composition is carried out by the method of free enthalpy minimization developed by Eriksson [1]. However, for open systems, the problem is not definitively solved yet. A computer code simulating the volatility of the elements present in an oxide system was developed by Pichelin [2] and Badie [3]. This computer code was modified by Ghiloufi to control the vaporization of the elements present in a chloride and oxide system during the fly ashes vitrification by plasma and to study the radioelement volatility during the treatment of radioactive wastes by thermal plasma [4-9].

In this chapter we present a method used in our computer code, which is developed to simulate and to modulate a chemical system vaporization at high temperature. This method is based on the calculation of composition by free energy minimization of the system, coupled with the mass transfer equation at the reactional interface. This coupling is ensured by fixing the equivalent partial pressure of oxygen in the mass transfer equation and those characterizing the complex balances.

This chapter contains five parts: In the first part we will present the method used to the calculation of composition by free energy minimization of a closed system, precisely we will develop the equations characterizing the complex balances at the reactional interface. In the second part we will give the mass transfer equation of oxygen. In the third part we will present the method used in our study to determine the diffusion coefficients of gas species essentially for complex molecules like vapor metals. In the fourth part we will apply the computer code to simulate the radioelement volatility during the vitrification of radioactive wastes by thermal plasma. In the last part we will present the results obtained by the computer code during the study of radioaelement volatility.

2. Description of the model

In the model, the species distribution in the liquid and gas phases is obtained iteratively using the calculation of system composition coupled with the mass transfer equation. The quantity of matter formed in the gas phase is distributed into three parts: The first part is in equilibrium with the bath, the second part is diffused in the diffusion layer, and the third part is retained by the bath under the electrolysis effects (Figure 1). The gas composition at the surface is thus modified. It is not the result of a single equilibrium liquid-gas, but instead, it is the outcome of a dynamic balance comprising: a combined action of reactional balances, electrolysis effects, and diffusive transport.

The flux density of a gas species *i* (J_i^L) lost in each iteration is given by:

$$J_i^L = J_i^D - J_i^R \tag{1}$$

Where J_i^D and J_i^R are, respectively, the diffusion flux density and the flux retained by the bath for the gas species *i*.

The vaporization model is applicable to several types of complex chemical systems. It is independent of the geometrical configuration of the vaporization system, but it is developed based on the following three hypotheses:

a. The chemical system consists of two phases: a vapor phase, whose species are regarded as perfect gases, and a homogeneous isothermal liquid phase.
b. The model is mono-dimensional: it does not introduce discretization on the variable space, but enables to calculate the composition of the two phases at each time interval.
c. The mass transfer at the interface is controlled by the gas species diffusion in the carrier gas because the reaction kinetics at the liquid/gas interface are very fast.

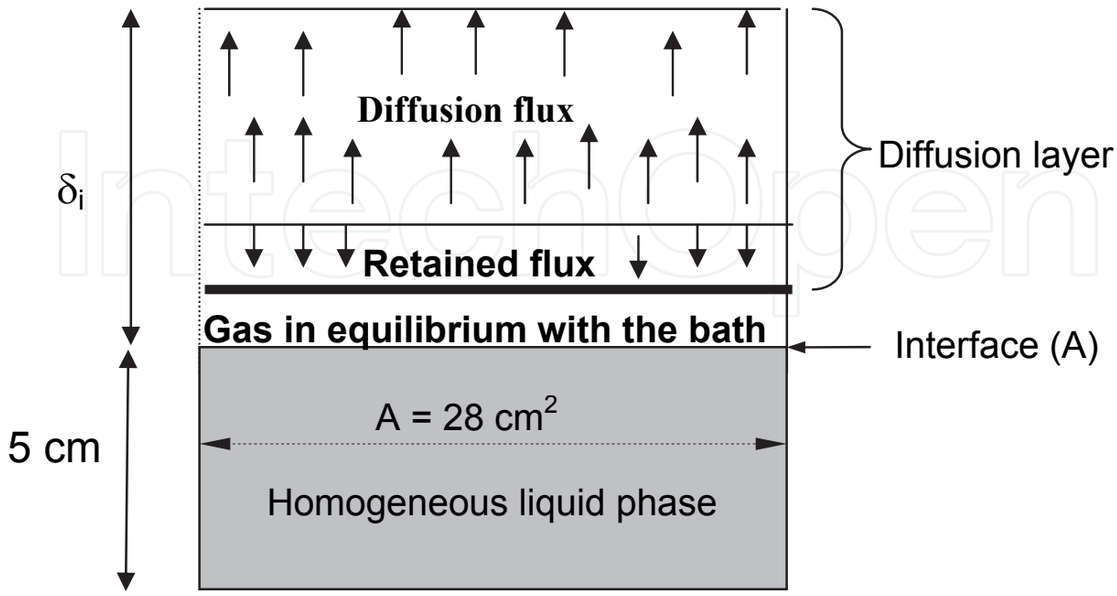

Fig. 1. Simplified diagram used to establish the assumptions of the model

3. Calculation of the gas/ liquid system composition

The free energy of a system made up of two phases; a vapor phase formed by Ml(1) species and a condensed phase consisting of Ml (2) species is as follows:

$$G = \sum_{i=1}^{Ml(1)} n_i \left(g_i^0 + RTLogp_i \right) + \sum_{i=Ml(1)+1}^{Ml(1)+Ml(2)} n_i \left(g_i^0 + RTLog\mathrm{X}_i \right) \tag{2}$$

where g_i^0 is the formation free enthalpy of a species under standard conditions, R is the perfect gas constant, T is the temperature, and n_i is the mole number of species *i*. The two terms p_i and X_i are, respectively, the partial pressure of a gas species, assumed a perfect gas, and the molar fraction of species *i* in the liquid phase assumed ideal.
Equation (2) can be written differently as:

$$F = \frac{G}{RT} = \sum_{i=1}^{Ml(1)} n_i \left[\frac{g_i^0}{RT} + LogP + Log \frac{n_i}{\bar{n}_g} \right] + \sum_{i=Ml(1)+1}^{Ml(1)+Ml(2)} n_i \left[\frac{g_i^0}{RT} + Log \frac{n_i}{\bar{n}_l} \right] \tag{3}$$

where P is the total pressure, $\bar{n}_g$ represents the total mole number of the species in the gas phase ($\bar{n}_g = \sum_{i=1}^{Ml(1)} n_i$) and $\bar{n}_l$ represents the total mole number of the species in the condensed phase ($\bar{n}_l = \sum_{i=Ml(1)+1}^{Ml(1)+Ml(2)} n_i$).

Let us assume that the system under study consists of L basic elements. Hence, the conservation of the elements mass results in:

$$\sum_{i=1}^{Ml(1)} a_{ij} n_i + \sum_{i=Ml(1)+1}^{Ml(1)+Ml(2)} a_{ij} n_i = B_j \quad j \in [1, L] \tag{4}$$

where a_{ij} is the atoms grams number of the element *j* in the chemical species *i* and B_j is the total number of atoms grams of the element *j* in the system.
The equivalent partial pressure of oxygen is given by:

$$P_{O2} = \frac{n_{O2}}{\bar{\bar{n}}_g} P \tag{5}$$

where n_{O2}, representing the equivalent mole number of oxygen, is given by:

$$n_{O2} = \sum_{i=1}^{Ml(1)} a_{iL} n_i \tag{6}$$

where a_{iL} is the atoms grams number of oxygen in the chemical species *i*. Combining (5) and (6) leads to:

$$\bar{n}_g \frac{P_{O2}}{P} = \sum_{i=1}^{Ml(1)} a_{iL} n_i \tag{7}$$

The calculation of the system composition to the balance coupled with the mass transfer equation, at constant temperature T and constant pressure P, consists of minimizing the function F under the constraints of (4) and (7). The Lagrange function becomes:

$$L(n_i) = \xi(n_i) + \sum_{j=1}^{L} \Pi_j \left(- \sum_{i=1}^{Ml(1)+Ml(2)} a_{ij} n_i + B_j \right) + \Pi_{L+1} \left(- \sum_{i=1}^{Ml(1)} a_{iL} n_i + \frac{P_{O2}}{P} \bar{n}_g \right) \tag{8}$$

where Π_j represents the Lagrange multipliers and the function ξ (n_i) is the Taylor series expansion of F (with orders higher than two being neglected).
To minimize F (ni) subject to (4) and (7), it is required to have:

$$\frac{\partial L}{\partial n_i} = 0 \quad \text{i=1,…,Ml(1)+Ml(2)} \tag{9}$$

$$\frac{\partial L}{\partial \Pi_j} = 0 \quad \text{j=1,…,L, L+1} \tag{10}$$

From (9), the expression of the mole number of a species *i* in the vapor phase or in the liquid phase can be deduced. That is to say:
For gases:

$$n_i = \left(-\frac{g_i^0}{RT} - LogP - Ln\left(\frac{n_i^0}{\bar{n}_g^0}\right) + \frac{\bar{n}_g}{\bar{n}_g^0} + \sum_{j=1}^{L} \Pi_j a_{ij} + \Pi_{L+1} \left(a_{iL} - \frac{P_{O2}}{P} \right)\right) n_i^0 \tag{11}$$

For liquid:

$$n_i = \left(-\frac{g_i^0}{RT} - Ln\left(\frac{n_i^0}{\bar{n}_l^0}\right) + \frac{\bar{n}_l}{\bar{n}_l^0} + \sum_{j=1}^{L} \Pi_j a_{ij}\right) n_i^0 \tag{12}$$

with $\bar{n}_g^0 = \sum_{i=1}^{Ml(1)} n_i^0$ and $\bar{n}_l^0 = \sum_{i=Ml(1)+1}^{Ml(1)+Ml(2)} n_i^0$

Substituting (11) and (12) in (10) results in a system of L+3 equations, whose unknown factors are the Lagrange multipliers (Π_1, Π_2,…, ΠL, Π_{L+1}), u_1, and u_2.

with $u_1 = \frac{\bar{n}_g}{\bar{n}_g^0} - 1$ and $u_2 = \frac{\bar{n}_l}{\bar{n}_l^0} - 1$.

Solving this set of equations then using (11) or (12), as needed, gives the values of n_i. These values n_i represent the improved values over the first iterations $n_i^{(1)}$. A loop of iterations is thus defined by using $n_i^{(k)}$ in the place of the n_i^{k-1} for the k^{th} iteration.

4. Transfer equation

4.1 Determination of the stoichiometric coefficient

To simplify the writing and calculation of the mass transfer equation at the interface, a dimensionless quantity X_j, called stoichiometric coefficient of a metal 'J', has been introduced and corresponding to :

$$X_j = \frac{n_{O-j}}{n_{M_j}} \tag{13}$$

where n_{O-j} is the mole number of oxygen in the liquid phase related to metal 'J', whereas the term n_{M_j} represents the total mole number of metal 'J' in the liquid phase, which contains m species. For example if N is the total mole number of metals in the mixing melted material, for an unspecified metal 'J', the expressions of X_j is as follows :

$$X_j = \frac{\sum_{i=1}^{m} a_{ik} n_i \dfrac{a_{ij}\upsilon_{ij}}{\sum_{j=1}^{N} a_{ij}\upsilon_{ij}}}{\sum_{i=1}^{m} a_{ij} n_i} \tag{14}$$

a_{ij} and a_{ik} are respectively the stoichiometric coefficients of the element 'J', and oxygen in species 'i'. n_i represents the number of moles of species 'i'. υ_{ij} is the valence of metal 'J' in oxide 'i'.

4.2 Example

In an initial mixture of Al-Si-Fe-O-Cl, for example, the species which can exist in the liquid phase at 1700 K are as follows: SiO_2, Fe_2SiO_4, Fe_3O_4, FeO, Al_2O_3, $AlCl_3$, $FeCl_2$. The iron stoichiometric coefficients X_{Fe} in the system is given by the following expression:

$$X_{Fe} = \frac{(4\, n_{Fe_2SiO_4} \times \frac{4}{8}) + 4\, n_{Fe_3O_4} + n_{FeO}}{2\, n_{Fe_2SiO_4} + 3\; n_{Fe_3O_4} + n_{FeO}} \tag{15}$$

4.3 Transfer equation

From equation (13), the oxygen mole number in the liquid phase related to metal 'J', can be deduced, i.e.

$$n_{O-j} = X_j . n_{M_j} \tag{16}$$

If equation (16) is differentiated relatively to time and each term is divided by the surface of the interface value A, it comes :

$$-\frac{1}{A}\frac{dn_{O-j}}{dt} = -\frac{1}{A} X_j \frac{dn_{M_j}}{dt} - \frac{1}{A} n_{M_j} \frac{dX_j}{dt} \tag{17}$$

The interfacial density of molar flux of a species 'i' is:

$$J_i = -\frac{1}{A}\frac{dn_i}{dt} \text{ (mole.s}^{-1}\text{.m}^{-2}\text{)} \tag{18}$$

Introducing equation (18), in equation (17), leads to:

$$(J_O^L)_{M_j} = \mathrm{X}_j.(J_{M_j}^L) - \frac{n_{M_J}}{A}\frac{d\mathrm{X}_j}{dt} \tag{19}$$

$(J_O^L)_{M_j}$ represent the surfacic molar flux densities of oxygen related to metal 'J' from the liquid phase, whereas $(J_{M_j}^L)$ is the equivalent density of molar flux of a metal J from the liquid phase.
The total surfacic densities of molar flux of oxygen from the liquid phase is expressed by:

$$(J_O^L) = \sum_{j=1}^{N}(J_O^L)_{M_j} \tag{20}$$

If in the equation (20) $(J_O^L)_{M_j}$ is replaced by its expression given by the equation (19) it follows:

$$(J_O^L) = \sum_{j=1}^{N}\mathrm{X}_j(J_{M_j}^L) - \frac{1}{A}\sum_{j=1}^{N}n_{M_j}.\frac{d\mathrm{X}_j}{dt} \tag{21}$$

Indicating by Ng, the number of species which can exist in the vapor phase, the expressions of the total densities of molar flux of oxygen and an unspecified metal 'J' in gas phase are:

$$(J_O^G) = \sum_{i=1}^{Ng}a_{ik}J_i^G \tag{22}$$

$$(J_{M_j}^G) = \sum_{i=1}^{Ng}a_{ij}J_i^G \tag{23}$$

where J_i^G is the molar flux density of a gas species 'i'.
The mass balance at the interfacial liquid to gas is expressed by the equality between the equivalent densities of molar flux of an element in the two phases, i.e. :

$$(J_i^L) = (J_i^G) \tag{24}$$

The use of matter conservation equations at the interface, for oxygen and metals, and the combination of equations (16), (17), (18), (19) and (20), lead to the following equation.

$$\sum_{j=1}^{N}X_j(J_{M_j}^G) - \sum_{i=1}^{Ng}a_{ik}J_i^G - \frac{1}{A}\sum_{j=1}^{N}n_{M_j}.\frac{dX_j}{dt} = 0 \tag{25}$$

The equation (25) is the oxygen matter conservation equation or the transfer equation at the interface. Argon is used as a carrier gas. In the plasma conditions, it is supposed that argon is an inert gas, so its molar flux density is zero:

$$J_{Ar}^{G} = 0 \tag{26}$$

The density flux for a gas species 'i' is given by:

$$J_i^G = -\frac{D_i}{RT}\left(\frac{p_i^x - p_i^w}{\delta_i}\right) + J_T.p_i^w \tag{27}$$

where p_i^w and p_i^x represent the interfacial partial pressure and the partial pressure in the carrier gas of species 'i' respectively; J_T is the total mass flux density with $J_T = \sum_{i=1}^{n-1} J_i^G$, $J_{Ar}^G = 0$ *and* $\sum_{i=1}^{n} p_i^w = 1atm$, δ_i is boundary layer thickness, and D_i is diffusion coefficient.

5. Flux retained by the bath

The Faraday's first law of electrolysis states that the mass of a substance produced at an electrode during electrolysis is proportional to the mole number of electrons (the quantity of electricity) transferred at that electrode [10]:

$$m = \frac{Q}{q\upsilon}\frac{M}{N_A} \tag{28}$$

where m is the mass of the substance produced at the electrode (in grams), Q is the total electric charge passing through the plasma (in coulombs), q is the electron charge, v is the valence number of the substance as an ion (electrons per ion), M is the molar mass of the substance (in grams per mole), and N_A is Avogadro's number. If the mole number of a substance i is initially n_i^0, its mole number produced at the electrode is:

$$n_i = \frac{Q}{qvN_A}n_i^0 \tag{29}$$

The interfacial density of molar flux of a species 'i' is:

$$J_i = \frac{1}{A}\frac{dn_i}{dt} \text{ (mole.s}^{-1}\text{.m}^{-2}\text{)} \tag{30}$$

The density (J_i^R), of molar flux of a species i retained by the bath under the electrolyses effects, can be obtained by substituting (29) in (30) to yield:

$$J_i^R = \frac{1}{A}\frac{dn_i}{dt} = \frac{1}{A}\frac{d\left(\frac{Q}{qvN_A}n_i^0\right)}{dt} = \frac{n_i^0}{A.qN_A.v}\frac{dQ}{dt} \tag{31}$$

$\frac{dQ}{dt} = I$ represents the current in the plasma and $F = qN_A = 96485\ C.mol^{-1}$ is Faraday's constant. Equation (31) becomes:

$$J_i^R = \frac{I}{A.F.v} n_i^0 \tag{32}$$

6. Numerical solution

Newton's numerical method solves the mass balance equations (26), (27) and (28) with respect to the interfacial thermodynamic equilibrium, the unknown parameters being the interfacial partial pressure P_i^w , the stoichiometric coefficient X_J and the molar flux densities J_i^G .

The convergence scheme is as follows:

- We calculate the liquid-gas interfacial chemical composition of the closed system by using Ericksson's program. The oxygen partial pressure is then defined by the convergence algorithm.
- The recently known values of p_i^w and X_J are introduced into the mass equilibrium equations which can be solved after a series of iterative operations up to the algorithm convergence.
- At the beginning of the next vaporization stage, the system is restarted with the new data of chemical composition. The time increment is not constant and should be adjusted to the stage in order to prevent convergence instabilities when a sudden local variation of the mass flux density occurs.

7. Estimation of the diffusion coefficients

Up to temperatures of about 1000 K, the binary diffusion coefficients are known for current gases, oxygen, argon, nitrogen…etc. For temperatures higher than 1000 K, the diffusion coefficients of the gas species in the carrier gas are calculated according to level 1 of the CHAPMAN-ENSKOG approximation [11]:

$$D_{ij} = 0.002628 \frac{\sqrt{T^3 (M_i + M_j) / 2M_i M_j}}{P\sigma_{ij}^2 \Omega_{ij}^{(1.1)^*}(T_{ij}^*)} \tag{33}$$

In this equation D_{ij} is the binary diffusion coefficient (in $cm^2.s^{-1}$) , M_i and M_j are the molar masses of species 'i' and 'j'. P is the total pressure (in atm), T is the temperature (in K), $T^* = T\frac{k}{\varepsilon_{ij}}$ is the reduced temperature, K is the Boltzmann constant, σ_{ij} is the collision diameter (in Å), ε_{ij} is the binary collision energy and $\Omega_{ij}^{(1.1)^*}(T^*)$ is the reduced collision integral.

For an interaction between two non-polar particles 'i' and 'j':

$$\varepsilon_{ij} = \sqrt{\varepsilon_i \varepsilon_j} \tag{34}$$

$$\sigma_{ij} = \frac{1}{2}\left(\sigma_i + \sigma_j\right) \tag{35}$$

The values relating to current gases needed for our calculations are those of Hirschfelder [11]. For the other gas species, such as the metal vapor, the parameters of the intermolecular potential remain unknown whatever the interaction potential used. This makes impossible the determination of the reduced collision integral. For this reason the particles are regarded as rigid spheres and the collision integrals are assimilated to those obtained with the rigid spheres model [12]. That is equivalent to the assumption:

$$\Omega_{ij}^{(1.1)^*}(T^*) = 1 \tag{36}$$

$$\sigma_{ij} = r_i + r_j \tag{37}$$

The terms r_i and r_j are the radii of the colliding particles. For the monoatomic particles, the atomic radii are already found. For the polyatomic particles, the radii of the complex molecules A_nB_m are unknown. Thus it has been supposed that they had a spherical form and their radii were estimated according to [12]:

$$r_{A_nB_m} = \left| n r_A^3 + m r_B^3 \right|^{1/3} \tag{38}$$

In the above expression, r_A and r_B are either of the ionic radius, or of the covalence radius according to the existing binding types. The radii of all the ions which form metal oxides and chlorides are extracted from the Shannon tables [13].
At high temperature (T > 1000 K), the D_{ij} variation law with the temperature is close to the power 3/2 [14]. For this reason the diffusion coefficients of the gas species are calculated with only one value of temperature (1700 K). For the other temperatures the following equation is applied:

$$D_{ij}(T_2) = D_{ij}(T_1).\left(\frac{T_2}{T_1}\right)^{3/2} \tag{39}$$

8. Application of the model

To simulate the same emission spectroscopy conditions in which the experimental measurement are obtained, the containment matrix used for this study is formed by basalt, and its composition is given in table 1.
At high temperatures (T > 1700K), in the presence of oxygen and argon, the following species are preserved in the model:

- In the vapor phase: O_2, O, Mg, MgO, K, KO, Na, Na_2, NaO, Ca, CaO, Si, SiO, SiO_2, Al, AlO, AlO_2, Fe, FeO, Ti, TiO, TiO_2, and Ar.
- In the condensed phase : $CaSiO_3$,Ca_2SiO_4, $CaMgSi_2O_6$, $K_2Si_2O_5$, SiO_2, Fe_2SiO_4, Fe_3O_4, FeO, $FeNaO_2$, Al_2O_3, CaO, Na_2O, Na_2SiO_3, $Na_2Si_2O_5$, K_2O, K_2SiO_3, MgO, $MgAl_2O_4$, $MgSiO_3$, Mg_2SiO_4, $CaTiSiO_5$, $MgTi_2O_5$, Mg_2TiO_4, $Na_2Ti_2O_5$, $Na_2Ti_3O_7$, TiO, TiO_2, Ti_2O_3, Ti_3O_5, and Ti_4O_7.

Elements	Mg	K	Na	Ca	Si	Al	Fe	Ti
Chemical form	MgO	K_2O	Na_2O	CaO	SiO_2	Al_2O_3	FeO	TiO_2
% in mass	10.2	1.2	3	8.8	50.4	12.2	11.9	2.2
Cation mole number	0.253	0.021	0.154	0.157	0.838	0.239	0.165	0.034

Table 1. Composition of basalt

This study focuses on the three radioelements ^{137}Cs, ^{60}Co, and ^{106}Ru. Ruthenium is a high activity radioelement, and it is an emitter of α, β and γ radiations, with long a radioactive period. However, Cesium and Cobalt are two low activity radioelements and they are emitters of β and γ radiations with short-periods on the average (less than or equal to 30 years) [15]. To simplify the system, the radioelements are introduced separately in the containment matrix, in their most probable chemical form. Table 2 recapitulates the chemical forms and the mass percentages of the radioelements used in the system. The mass percentages chosen in this study are the same as that used in experimental measurements made by [9, 16].

radioelement	^{137}Cs	^{60}Co	^{106}Ru
Most probable chemical form	Cs_2O	CoO	Ru
% in mass	10	10	5

Table 2. Chemical Forms and Mass Percentages of radioelement

The addition of these elements to the containment matrix, in the presence of oxygen, leads to the formation of the following species:

- In the vapor phase: Cs, Cs_2, CsK, CsNa, CsO, Cs_2O, Cs_2O_2, Ru, RuO, RuO_2, RuO_3, RuO_4, Co, Co_2, and CoO.
- In the condensed phase: Cs, Cs_2O, Cs_2O_2, Cs_2SiO_3, $Cs_2Si_2O_5$, $Cs_2Si_4O_9$, Ru, CoAl, CoO, Co_2SiO_4, CoSi, $CoSi_2$, Co_2Si, and Co.

These species are selected with the assistance of the HSC computer code [17]. In the simulation, the selected formation free enthalpies of species are extracted from the tables of [18-20].

9. Simulation results

In this part we will present only the results of radioelement volatility obtained by our computer code during the treatment of radioactive wastes by plasma. However the results of heavy metal volatility during fly ashes treatment by thermal plasma can be find in [4,5].

9.1 Temperature influence

To have the same emission spectroscopy conditions in which the experimental measurement are obtained [9, 16], in this study the partial pressure of oxygen in the carrier gas P_{O_2} is fixed at 0.01 atm, the total pressure P at 1 atm, and the plasma current I at 250 A. Figures 2 and 3 depict respectively, the influence of bath surface temperatures on the Cobalt and Ruthenium volatility. Up to temperatures of about 2000 K, Cobalt is not volatile. Beyond this

value, any increase of temperature causes a considerable increase in both the vaporization speed and the vaporized quantity of ^{60}Co. This behavior was also observed for ^{137}Cs [8]. Contrarily to Cobalt, Ruthenium has a different behavior with temperature. For temperatures less than 1700 K and beyond 2000 K, Ruthenium volatility increases whith temperature increases. Whereas in the temperature interval between 1700 K and 2000 K, any increase of temperature decreases the ^{106}Ru volatility.
To better understand this Ru behavior, it is necessary to know its composition at different temperatures. Table 3 presents the mole numbers of Ru components in the gas phase at different temperatures obtained from the simulation results.

	species	Ru	RuO	RuO_2	RuO_3	RuO_4
Mole numbers	1700K	6.10^{-14}	3.10^{-10}	4.10^{-6}	7.10^{-5}	1.10^{-6}
	2000K	5.10^{-11}	2.10^{-8}	1.10^{-5}	3.10^{-5}	1.10^{-7}
	2500K	1.10^{-7}	2.10^{-6}	8.10^{-5}	1.10^{-5}	2.10^{-8}

Table 3. Mole numbers of Ru components in the gas phase at different temperatures

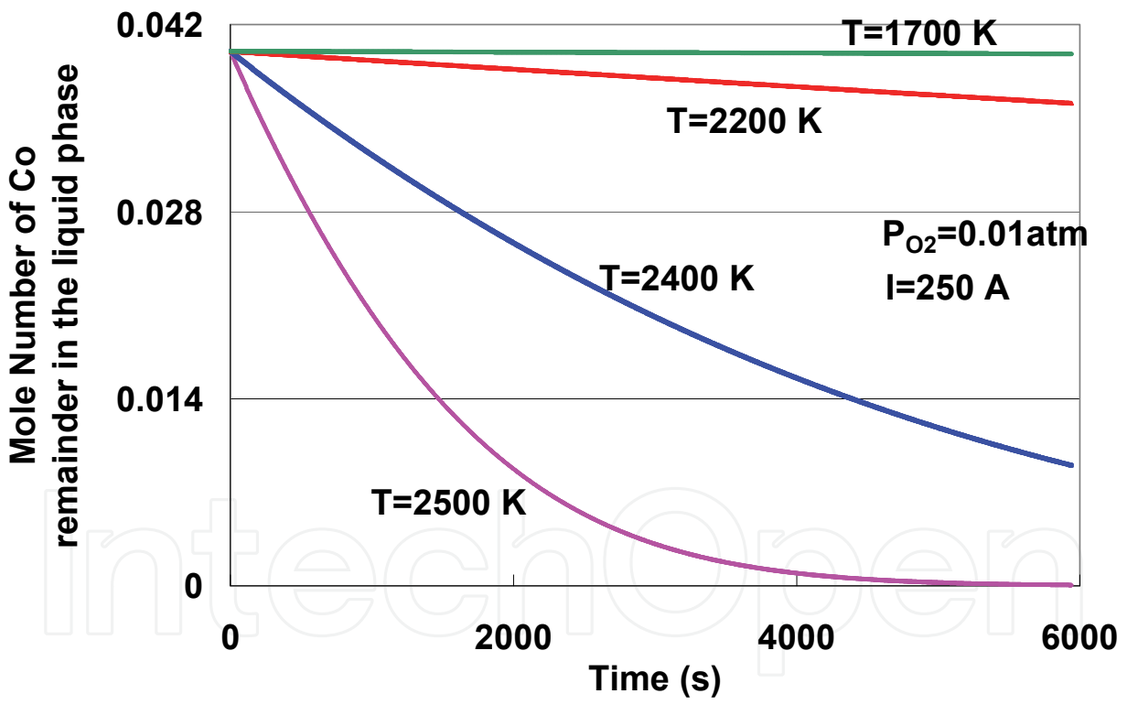

Fig. 2. Influence of temperature on Co volatility

The first observation that can be made is that the mole numbers of Ru, RuO, and RuO_2 increase with temperature, contrary to RuO_3 and RuO_4 whose mole numbers decrease with increasing temperatures. These results are logical because the formation free enthalpies of Ru, RuO, and RuO_2 decrease with temperature. Therefore, these species become more stable when the temperature increases, while is not the case for RuO_3 and RuO_4. A more interesting observation is that at temperatures between 1700 and 2000 K the mole numbers of Ru, RuO, and RuO_2 increase by an amount smaller that the amount of decrease of the

mole numbers of RuO_3 and RuO_4 resulting in an overall reduction of the total mole numbers formed in the gas phase. At temperature between 2000 and 2500 K the opposite phenomenon occurs.

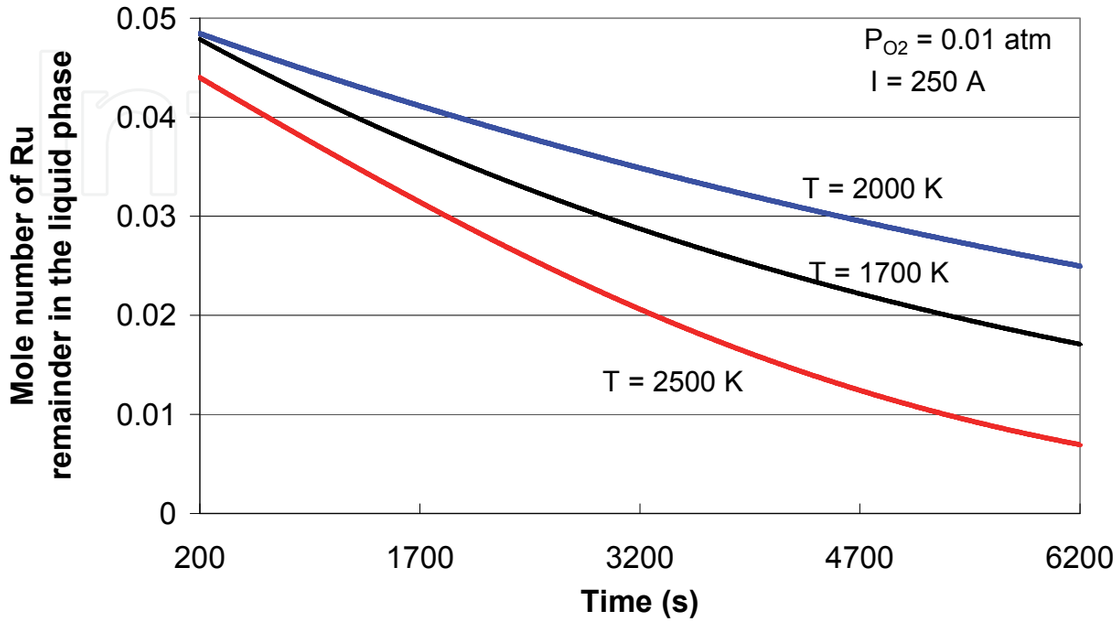

Fig. 3. Influence of temperature on Ru volatility

9.2 Effect of the atmosphere

The furnace atmosphere is supposed to be constantly renewed with a composition similar to that of the carrier gas made up of the mixture argon/oxygen. For this study, the temperature is fixed at 2500 K, the total pressure P at 1 atm and the plasma current I at 250 A. Figures 4 and 5 present the results obtained for ^{60}Co and ^{106}Ru as a function of P_{O_2}.

For ^{60}Co, a decrease in the vaporization speed and in the volatilized quantity can be noticed when the quantity of oxygen increases, i.e., when the atmosphere becomes more oxidizing. The presence of oxygen in the carrier gas supports the incorporation of Cobalt in the containment matrix. The same behavior is observed in the case of ^{137}Cs in accordance with P_{O_2} [8].

When studying the Ruthenium volatility presented in the curves of figure 5 it is found that, contrary to ^{60}Co, this volatility increases with the increase of the oxygen quantity. This difference in the Ruthenium behavior compared to Cobalt can be attributed to the redox character of the majority species in the condensed phase and gas in equilibrium. For ^{60}Co, the oxidation degree of the gas species is smaller than or equal to that of the condensed phase species, hence the presence of oxygen in the carrier gas supports the volatility of ^{60}Co. Whereas ^{106}Ru, in the liquid phase, has only one form (Ru). Hence, the oxidation degree of the gas species is greater than or equal to that of liquid phase species and any addition of oxygen in the gas phase increases its volatility.

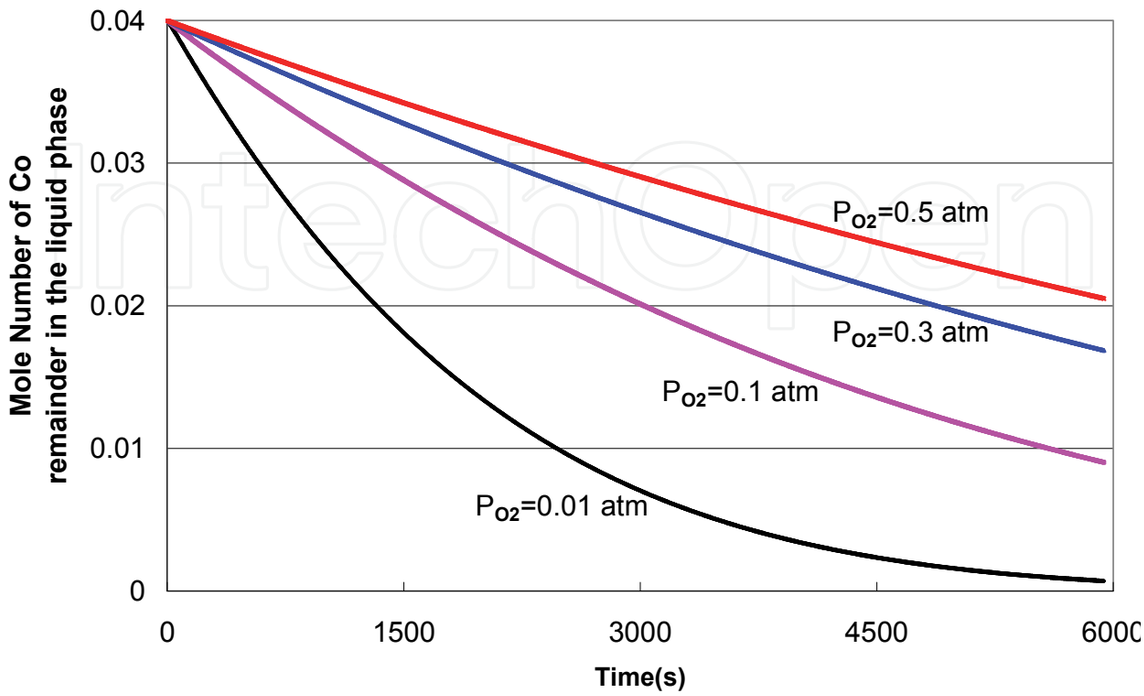

Fig. 4. Influence of the atmosphere nature on the Co volatility

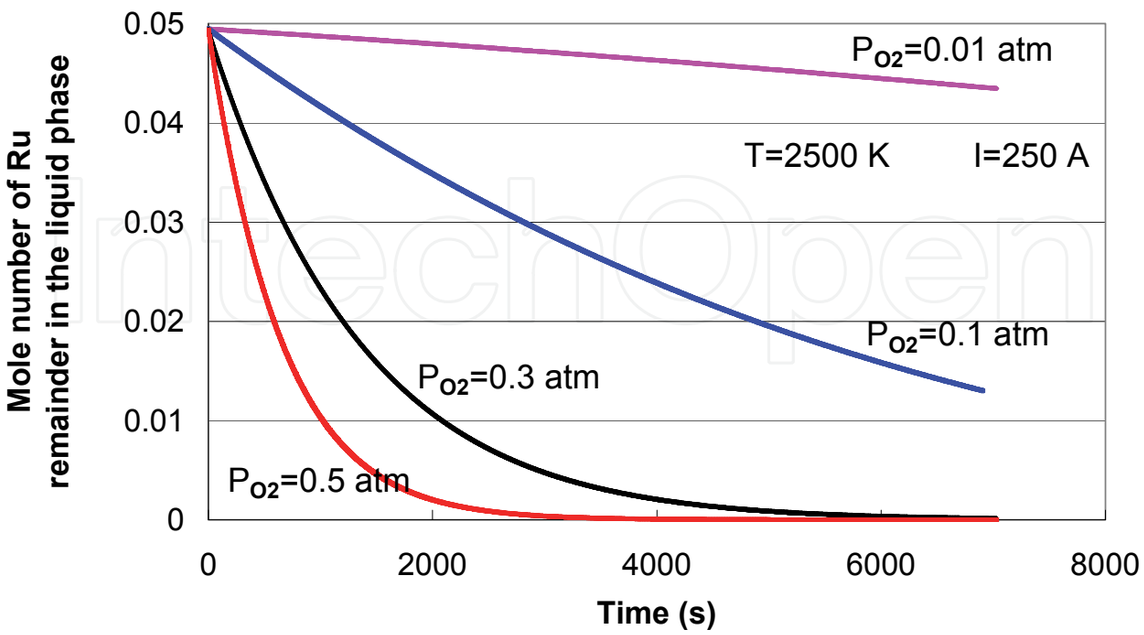

Fig. 5. Influence of the atmosphere nature on the Ru volatility

9.3 Influence of current

To study the influence of the current on the radioelement volatility, the temperature and the partial pressure of oxygen are fixed, respectively, at 2200 K and at 0.2 atm, whereas the plasma current is varied from 0 A to 600 A. Figures 6 and 7 depict the influence of plasma

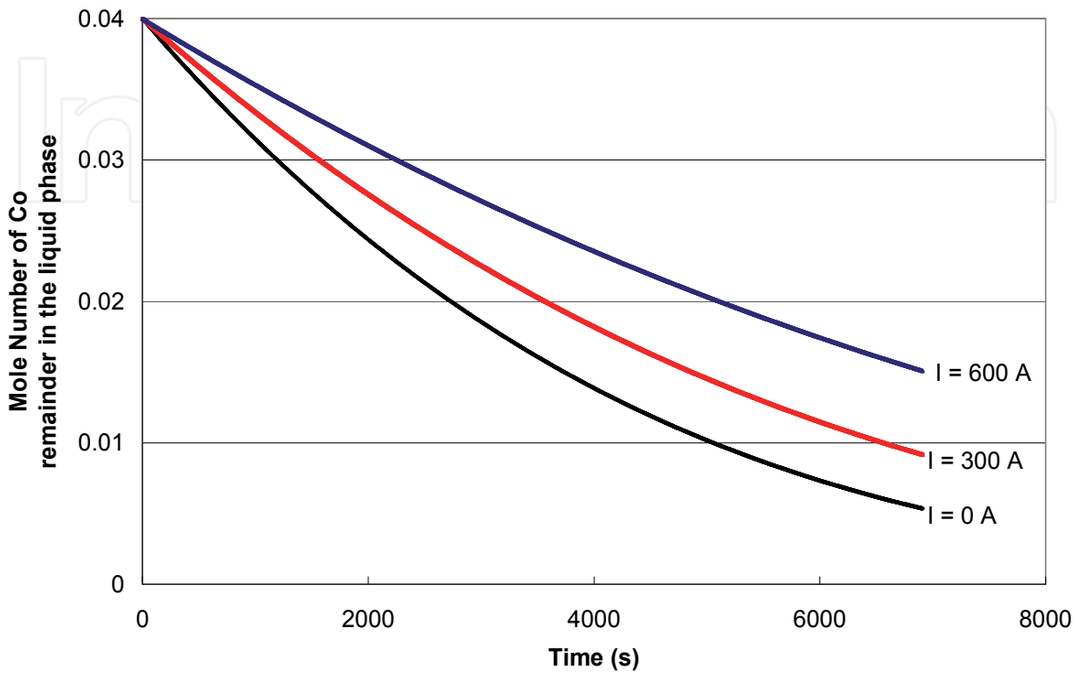

Fig. 6. Influence of plasma current on Co volatility

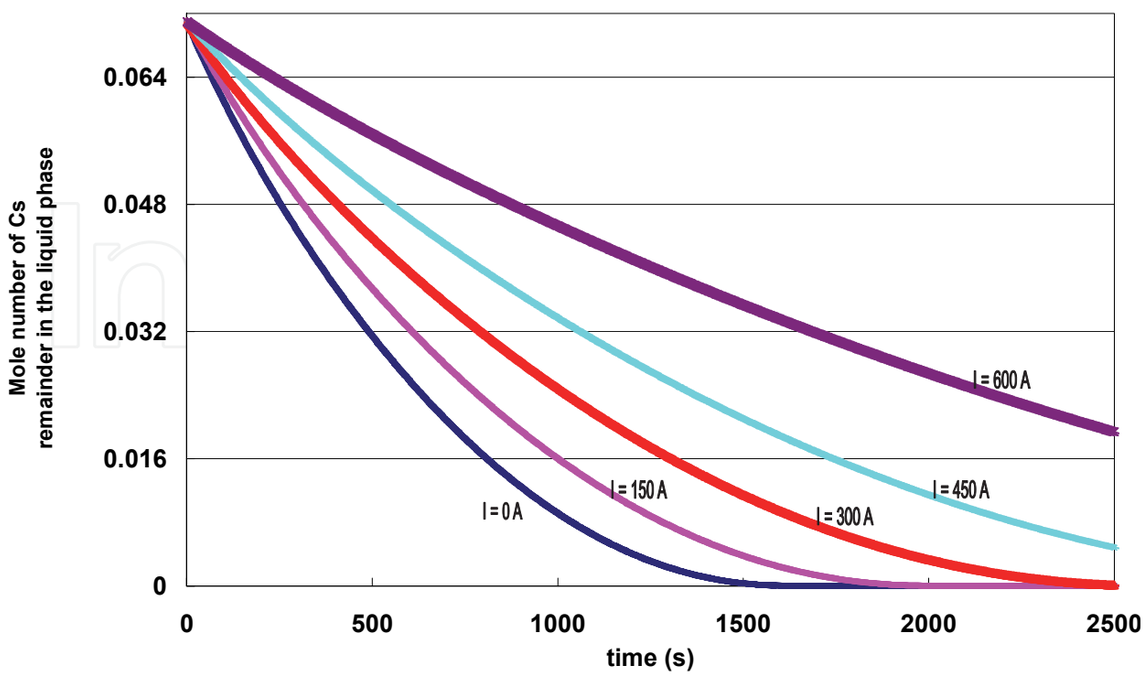

Fig. 7. Influence of current on Cs volatility

current on the Cobalt and Cesium volatility. The curves of these figures indicate that the increase of the plasma current considerably increases both the vaporization speed and the vaporized quantity of ^{60}Co and ^{137}Cs.
In the model, the electrolyses effects are represented by the ions flux retained by the bath, given by equation (32), which depends essentially on the plasma current. As the evaporation kinetics decrease with intensity current, the bath is in cathode polarization which prevents ^{60}Co and ^{137}Cs from leaving the liquid phase. Theses results assert the validity of equation (32) used by this computer code and conforms to the experimental results obtained by spectroscopy emission [9, 16]. The same behavior is observed in the case of ^{106}Ru as a function of plasma current.

9.4 Influence of matrix composition

Three matrices are used in this study and their compositions are given in table 4. Matrix 1 is obtained by the elimination of 29 g of Silicon for each 100 g of basalt, whereas matrix 2 is obtained by the addition of 65 g of Silicon for each 100 g of basalt, and matrix 3 is basalt. Figures 8 and 9 depict the influence of containment matrix composition, respectively, on the Cobalt and Cesium volatility. The increase of silicon percentage in the containment matrix supports the incorporation of ^{60}Co and ^{137}Cs in the matrix.
For ^{137}Cs, the increase of silicon percentage in the containment matrix is accompanied by an increase in mole numbers of $Cs_2Si_2O_5$ and $Cs_2Si_4O_9$ in the condensed phase. The presence of these two species in addition to Cs_2SiO_3 in significant amounts (between 10^{-3} and 10^{-2} mole) prevents Cs from leaving the liquid phase and reduces its volatility. For Cobalt, the increase of silicon percentage in the system supports the confinement of ^{60}Co in the condensed phase in the Co_2SiO_4 form. Ruthenium is not considered in this study because, in the liquid phase, it has only the Ru form and any modification in the containment matrix has no effect on its volatility.

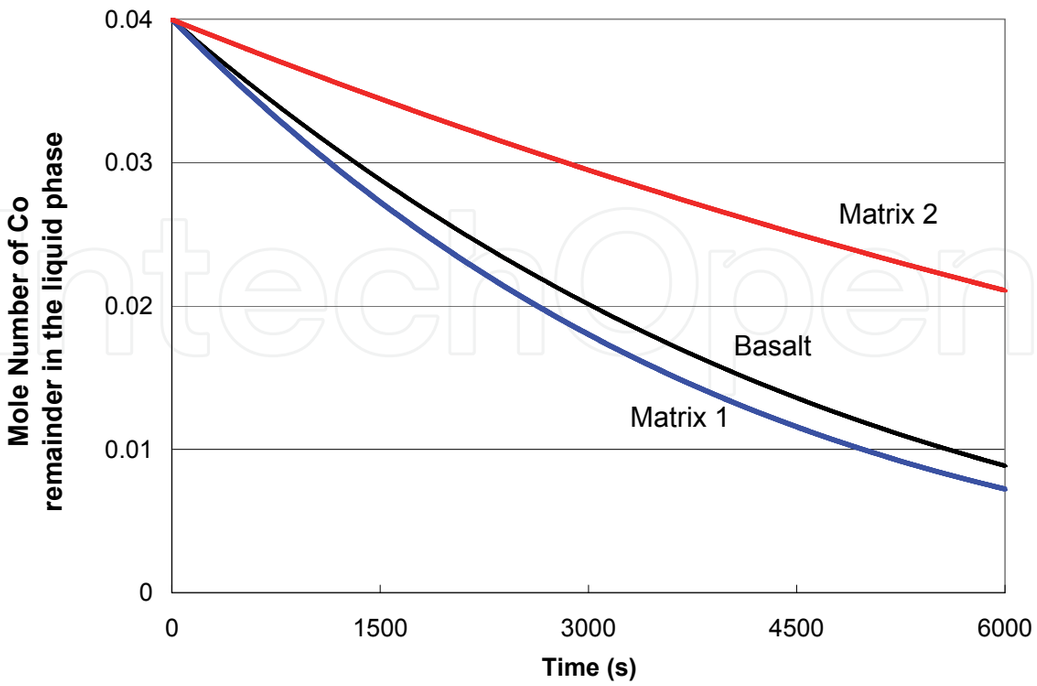

Fig. 8. Influence of matrix composition on Co volatility

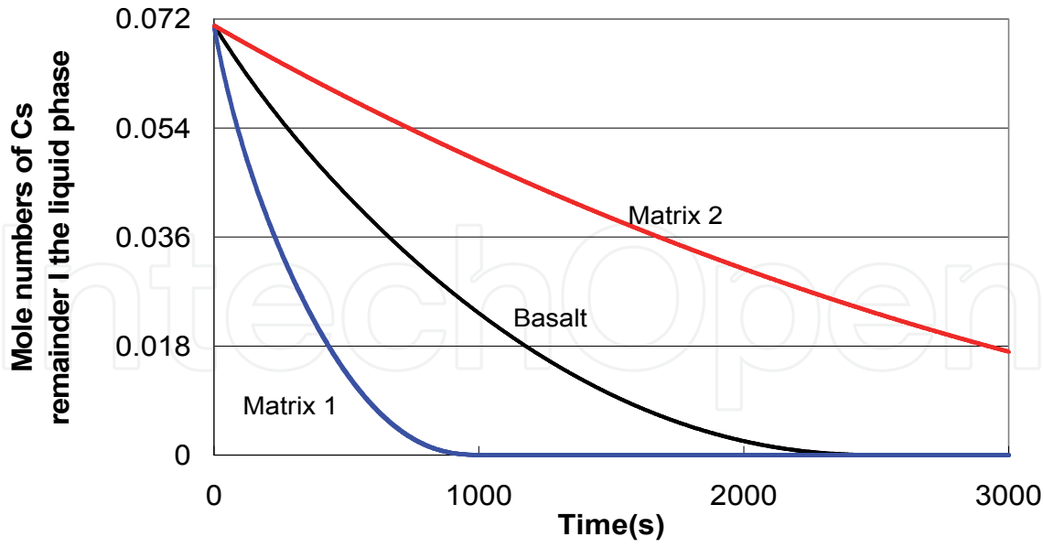

Fig. 9. Influence of matrix composition on Cs volatility

9.5 Distribution of Co and Ru on its elements during the treatment

Figures 10 and 11 depict the distribution of Cobalt components on the liquid and gas phases. In the gas phase, Cobalt exists essentially in the form of Co and, to a smaller degree, in the CoO form. In the liquid phase, Cobalt is found in quasi totality in CoO, Co and Co_2SiO_4 forms. Figure 12 presents the distribution of Ruthenium components on the liquid and gas phases. In the gas phase, Ruthenium exists essentially in the form of RuO_2 and, to a smaller degree, in the form of RuO_3 and RuO, whereas Ru and RuO_4 exist in much smaller quantities compared to the other forms. In the liquid phase, Ruthenium has only the Ru form.

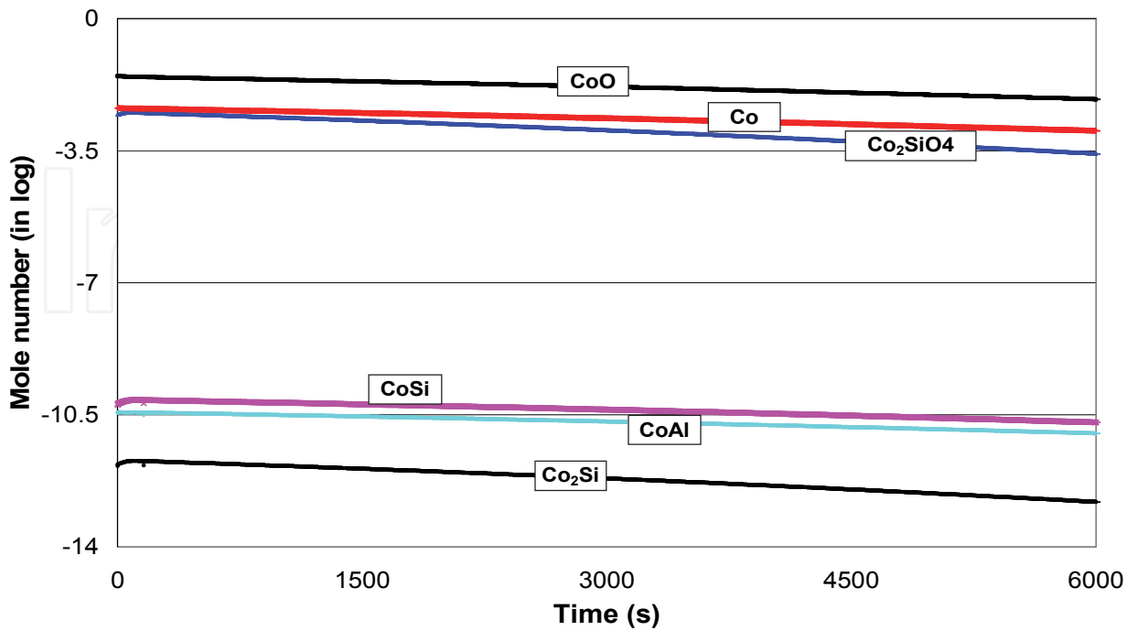

Fig. 10. Variation of the mole numbers of Co composition in the gas phase

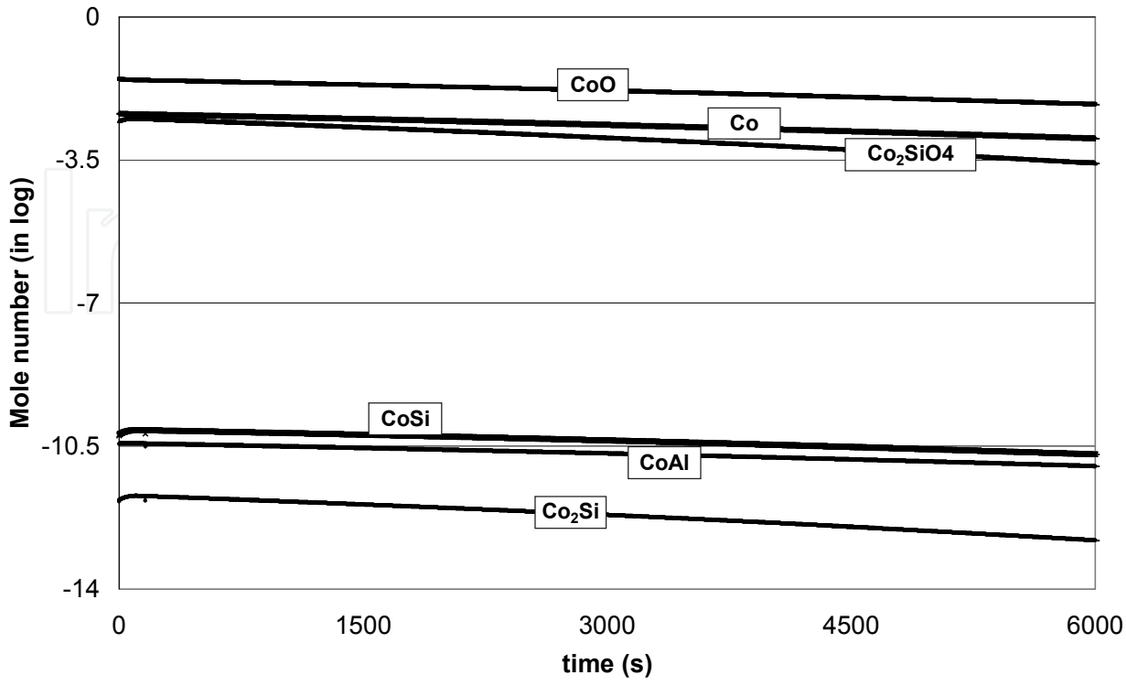

Fig. 11. Variation of the mole numbers of Co composition in the liquid phase

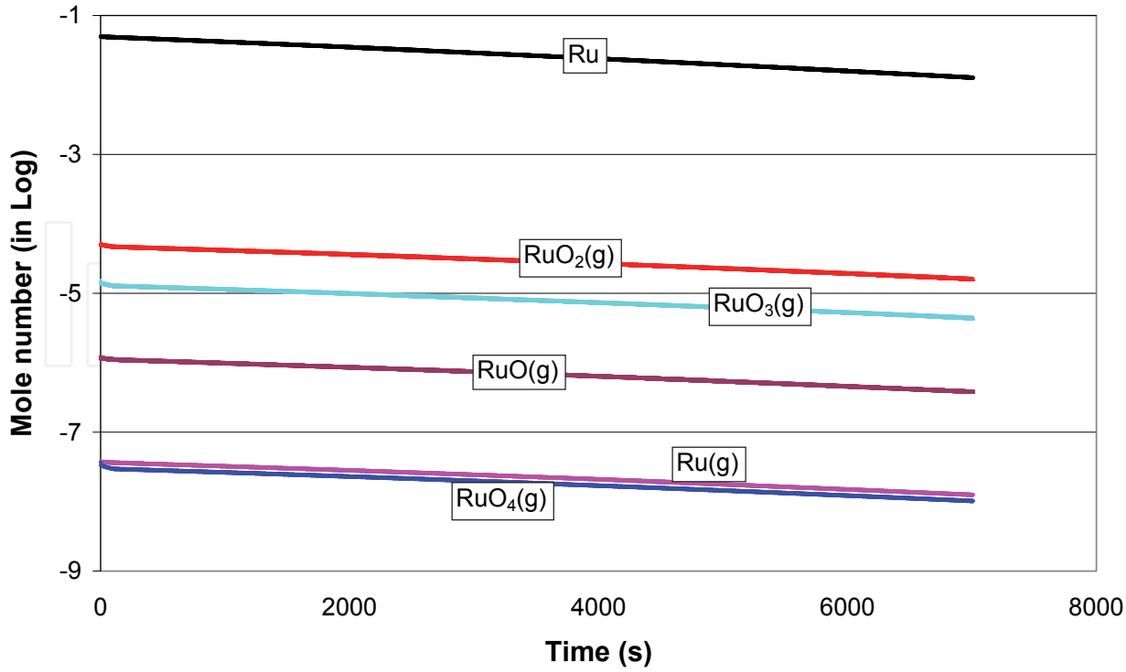

Fig. 12. Variation of the mole numbers of Ru composition in the gas and liquid phases

10. Comparison with the experimental results

The experimental setup is constituted of a cylindrical furnace, which supports a plasma device with twin-torch transferred arc system. The two plasma torches have opposite polarity. The reactor and the torches are cooled with water under pressure by two completely independent circuits. Argon is introduced at the tungsten cathode and the copper anode while oxygen, helium and hydrogen are injected through a water-cooled pipe [21]. To perform spectroscopic diagnostic above the molten surface, a water cooled stainless-steel crucible is placed under the coupling zone of the twin plasma torches. This crucible is filled with basalt and 10 % in oxide mass of Cs. On the cooled walls, the material does not melt and, hence, runs as a self-crucible. The intensities of the Ar line (λ = 667.72 nm) and the Cs line (λ = 672.32 nm) are measured by using an optical emission spectroscopy method (figure 13). The molar ratio Cs/Ar is deduced from the intensity ratio of the two lines [9, 16].

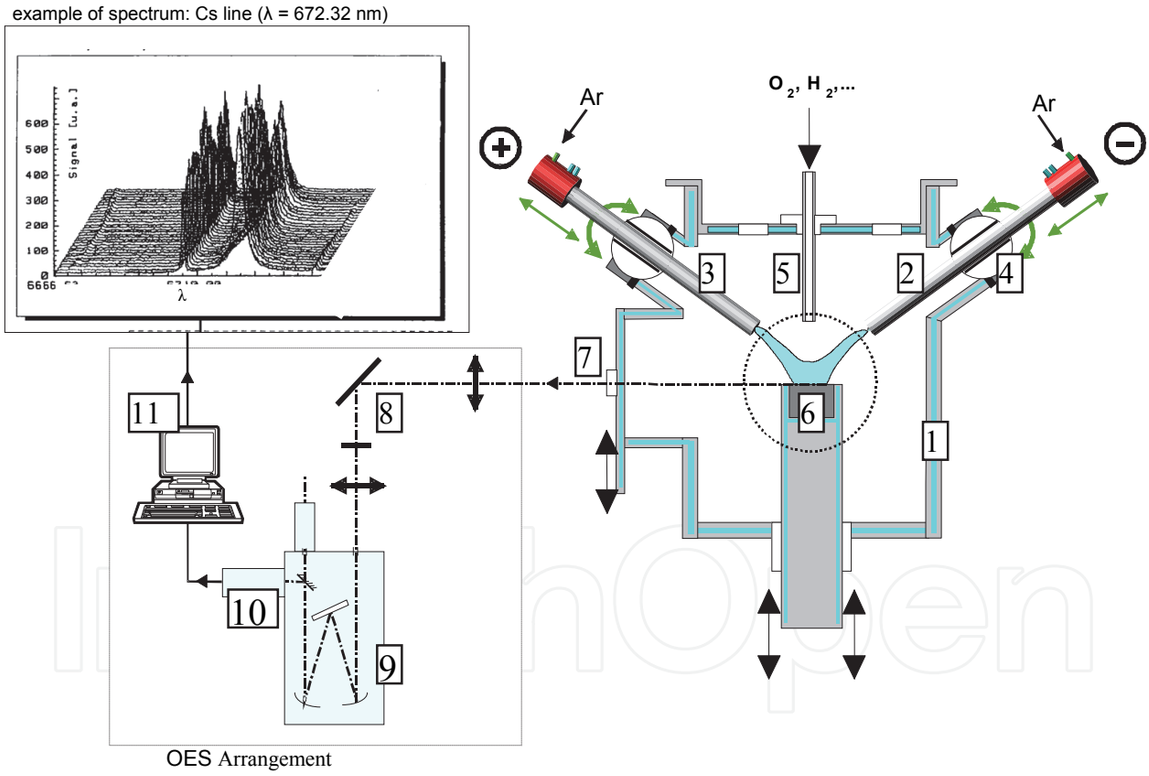

Fig. 13. Schematic of the experimental setup: (1) reactor vessel; (2) cathode torch; (3) anode torch; (4) spherical-bearing arrangement; (5) injection lance; (6) crucible; (7) porthole; (8) optical system; (9) monochromator; (10) OMA detector; (11) computer.

Figure 14 shows the code results in comparison with the experimental measurements. This figure reveals that the experimental and simulation results are relatively close. The

small difference between the simulation results and the experimental measurements can be attributed to the measurements errors. In fact, the estimated error committed on the measurement of the ratio Cs/Ar is around 10% [9, 16]. The model calculations assumed a bath fully melted and homogeneous from the beginning (t = 0s), while in practice the inside of the crucible is not fully melted and there is a progress of fusion front that allows a permanent alimentation of the liquid phase in elements from the solid. These causes explain the perturbation of the experimental measurements and the large gap between these measurements and the results obtained by the model in the first few minutes.

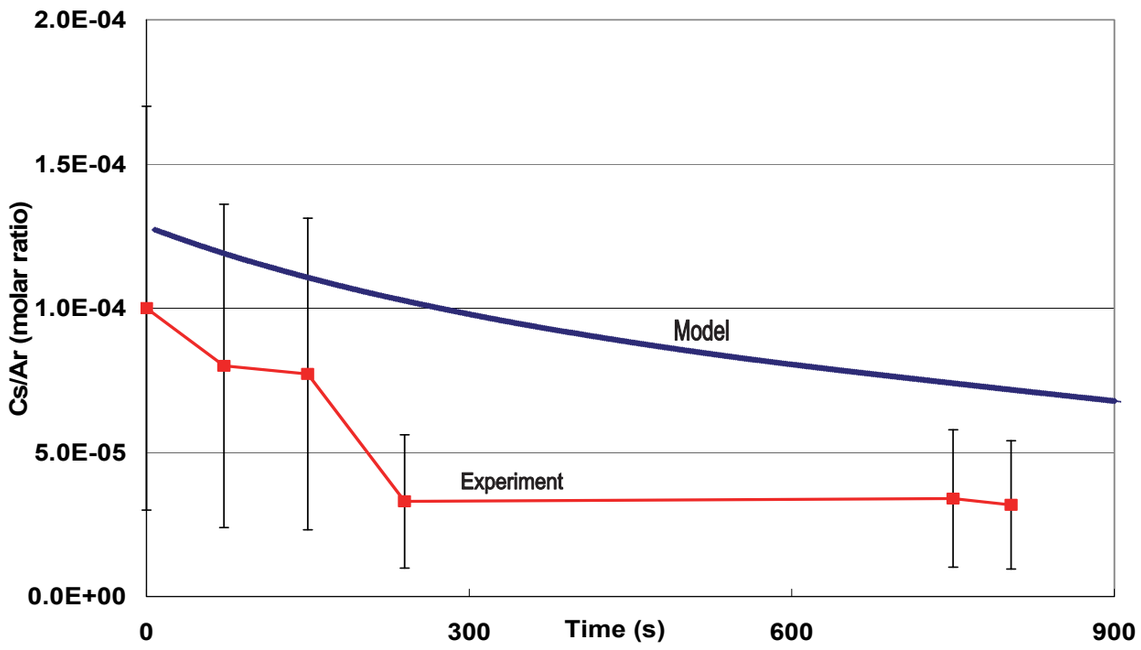

Fig. 14. Comparison between the simulation and experimental results in the case of Cs

11. Conclusion

The objective of this method is to improve the evaporation phenomena related to the radioelement volatility and to examine their behavior when they are subjected to a heat treatment such as vitrification by arc plasma. The main results show that up to temperatures of about 2000 K, Cobalt is not volatile. For temperatures higher than 2000 K, any increase in molten bath temperature causes an increase in the Cobalt volatility. Ruthenium, however, has a different behavior with temperature compared to Cobalt. For temperatures less than 1700 K and beyond 2000 K, Ruthenium volatility increases when temperature increases. Whereas in the temperature interval from 1700 K to 2000 K, any increase of temperature decreases the Ru volatility. Oxygen flux in the carrier gas supports the radioelement incorporations in the containment matrix, except in the case of the Ruthenium which is more volatile under an oxidizing atmosphere. For electrolyses

effects, an increase in the plasma current considerably increases both the vaporization speed and the vaporized quantities of Cs and Co. The increase of silicon percentage in the containment matrix supports the incorporation of Co and Cs in the matrix. The comparison between the simulation results and the experimental measurements reveals the adequacy of the computer code.

12. Acknowledgements

This work was supported by the National Plan, for Sciences, Technology and innovation, at Al Imam Muhammed Ibn Saud University, college of Sciences, Kingdom of Saudi Arabia.

13. Nomenclature

J_i^D :	diffusion flux density for the gas species *i*.
J_i^R :	flux retained by the bath for the gas species *i*.
G:	free energy of a system
g_i^0 :	formation free enthalpy of a species under standard conditions,
R :	perfect gas constant,
T :	temperature,
n_i :	mole number of species *i*.
p_i :	partial pressure of a gas species
X_i :	molar fraction of species *i* in the liquid phase.
P :	total pressure,
$\bar{n}_g$:	total mole number of the species in the gas phase,
$\bar{n}_l$:	total mole number of the species in the condensed phase
a_{ij} :	atoms grams number of the element *j* in the chemical species *i*
B_j :	total number of atoms grams of the element *j* in the system.
n_{O2}:	equivalent mole number of oxygen
L:	Lagrange function
$\prod_j$:	Lagrange multipliers
ξ (n_i) :	Taylor series expansion of F (F=G/RT)
$n_{O\text{-}j}$:	mole number of oxygen in the liquid phase related to metal 'J'
n_{M_j} :	total mole number of metal 'J' in the liquid phase
υ_{ij} :	valence of metal 'J' in oxide 'i'
A:	value of interface surface
J_i :	interfacial density of molar flux of a species 'i'
δ_i :	boundary layer thickness
D_i :	diffusion coefficient
m :	mass of the substance produced at the electrode
Q :	total electric charge passing through the plasma
q :	electron charge
v :	valence number of the substance as an ion (electrons per ion)

M : molar mass of the substance
N_A : Avogadro's number
I: current in the plasma
F: Faraday's constant
$T^* = T\frac{k}{\varepsilon_{ij}}$: reduced temperature
K : Boltzmann constant
σ_{ij}: collision diameter
ε_{ij} : binary collision energy
$\Omega_{ij}^{(1.1)^*}(T^*)$: reduced collision integral
r_i : radius of a particle

14. References

[1] Eriksson G., Rosen E., J. Chemica Scripta, 4:193, (1973)
[2] Pichelin G., Rouanet A., *J. Chemical Engineering Science,* 46:1635, (1991)
[3] Badie J. M., Chen X., Flamant G., *J. Chemical Engineering Science,* 52:4381, (1997)
[4] Ghiloufi I., Baronnet J. M., *J. High Temperature Materials Process,* volume 10, Issue 1, p. 117-139, (2006)
[5] Ghiloufi I., *J. High Temperature Materials Process,* volume12, Issue1, p.1-10, (2008)
[6] Ghiloufi, I., *J. Hazard. Mater.* 163, 136-142, (2009)
[7] Ghiloufi, I., *J. Plasma Chemistry and Plasma Processing,* Volume 29, Number 4 321-331, (2009)
[8] Ghiloufi I., Amouroux J., *J. High Temperature Materials Process,* volume 14, Issue 1, p. 71-84, (2010)
[9] Ghiloufi I., Girold C., *J. Plasma Chemistry and Plasma Processing,* 31:109–125, (2011)
[10] Serway, Moses, and Moyer, *Modern Physics*, third edition (2005)
[11] Hirschfelder, J. O., Curtis, C. F., and Bird, R. B., (1954), *Molecular Theory of Gases and Liquids*, John Willey & Sons, New-York.
[12] Razafinimanana, M., (1982), "Etude des coefficients de transport dans les mélanges hexafluorure de soufre azote application à l'arc électrique", Thèse, Université de Toulouse.
[13] Shannon R. D., Prewitt C. T., (1969), "Effective Ionic Radii Oxides and Fluorides", Acta Cryst., Vol. B25, pp. 925-946.
[14] Bird R. B., Stewart W. E., Lightfood E. N., (1960): "Transport phenomena" Ed. Willy.
[15] M. Jorda, E. Revertegat, Les clefs du CEA, n◦30, 1995, pp. 48–61.
[16] C. Girold, Incinération/vitrification de déchets radioactifs et combustion de gaz de pyrolyse en plasma d'arc, Ph.D. Thesis, Université de Limoges, France, 1997.
[17] Outokumpu HSC Chemistry, Chemical Reaction and Equilibrium Modules with Extensive Thermochemical Database, Version 6, (2006)
[18] Barin I., Thermochemical Data of Pure Substances, Weinheim; Basel, Switzerland; Cambridge; New York: VCH, (1989)

[19] Chase Malcolm, NIST-JANAF, Thermochemical Tables, Fourth Edition, J. of Phys. and Chem. Ref. Data, Monograph No. 9, (1998)
[20] Landolt-Bornstein, Thermodynamic Properties of Inorganic Material, Scientific Group Thermodata Europe (SGTE), Springer-Verlag, Berlin-Heidelberg, (1999)
[21] S. Megy, S. Bousrih, J.M.,Baronnet, E.A. Ershov-Pavlov, J.K. Williams, D.M. Iddles, J. Plasma Chemistry and Plasma Processing, 15, n° 2, (1995), 309 - 319.

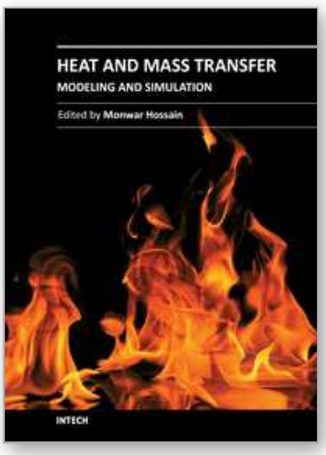

Heat and Mass Transfer - Modeling and Simulation

Edited by Prof. Md Monwar Hossain

ISBN 978-953-307-604-1
Hard cover, 216 pages
Publisher InTech
Published online 22, September, 2011
Published in print edition September, 2011

This book covers a number of topics in heat and mass transfer processes for a variety of industrial applications. The research papers provide advances in knowledge and design guidelines in terms of theory, mathematical modeling and experimental findings in multiple research areas relevant to many industrial processes and related equipment design. The design of equipment includes air heaters, cooling towers, chemical system vaporization, high temperature polymerization and hydrogen production by steam reforming. Nine chapters of the book will serve as an important reference for scientists and academics working in the research areas mentioned above, especially in the aspects of heat and mass transfer, analytical/numerical solutions and optimization of the processes.

InTech Europe
University Campus STeP Ri
Slavka Krautzeka 83/A
51000 Rijeka, Croatia
Phone: +385 (51) 770 447
Fax: +385 (51) 686 166
www.intechopen.com

InTech China
Unit 405, Office Block, Hotel Equatorial Shanghai
No.65, Yan An Road (West), Shanghai, 200040, China
中国上海市延安西路65号上海国际贵都大饭店办公楼405单元
Phone: +86-21-62489820
Fax: +86-21-62489821

IntechOpen